Collection and focusing of laser accelerated ion beams for therapy applications

Ingo Hofmann*
Helmholtz-Institut Jena, Helmholtzweg 4, 07743 Jena, Germany

Jürgen Meyer-ter-Vehn and Xueqing Yan†
Max-Planck-Institut für Quantenoptik, Hans-Kopfermann-Straße 1, 85748 Garching, Germany

Anna Orzhekhovskaya and Stepan Yaramyshev
Gesellschaft für Schwerionenforschung (GSI), Planckstraße 1, 64291 Darmstadt, Germany
(Received 20 December 2010; published 23 March 2011)

Experimental results in laser acceleration of protons and ions and theoretical predictions that the currently achieved energies might be raised by factors 5–10 in the next few years have stimulated research exploring this new technology for oncology as a compact alternative to conventional synchrotron based accelerator technology. The emphasis of this paper is on collection and focusing of the laser produced particles by using simulation data from a specific laser acceleration model. We present a scaling law for the ''chromatic emittance'' of the collector—here assumed as a solenoid lens—and apply it to the particle energy and angular spectra of the simulation output. For a 10 Hz laser system we find that particle collection by a solenoid magnet well satisfies requirements of intensity and beam quality as needed for depth scanning irradiation. This includes a sufficiently large safety margin for intensity, whereas a scheme without collection—by using mere aperture collimation—hardly reaches the needed intensities.

DOI: 10.1103/PhysRevSTAB.14.031304 PACS numbers: 41.75.Jv, 87.56.J−

I. INTRODUCTION

Proton and ion acceleration by irradiating thin foils with very high power laser beams and the observation of up to 60 MeV protons [1–3] have triggered suggestions that this principle might lend itself to a new technology for tumor therapy. Lasers would then have to compete with conventional accelerator technologies—synchrotrons or cyclotrons—and their high standard achieved in more than half a century of development.

The use of both protons and the biologically more effective carbon ions is currently done with synchrotrons (historically first at Berkeley, and currently at Tokyo and Heidelberg, with others under construction). Because of the higher magnetic rigidity of 400 MeV/u C^{6+} compared with protons of 250 MeV, they have typical diameters of 20–30 m. Synchrotrons are highly suitable for advanced scanning techniques, which allow a three-dimensional target-conformal treatment by using the active energy variation of the synchrotron accelerator combined with lateral scanning deflection using magnets [4].

Parameters of the recently built Heidelberg Ion Therapy (HIT) facility are used here as reference [5]. In HIT maximum flexibility is realized with the treatment of small as well as large in-depth tumor volumes requiring the maximum energy of 250 MeV for protons and 440 MeV/u for carbon. Specific differences for laser ions are the much higher production energy spread compared with the synchrotron case and the choice of laser pulse repetition rate assumed here as 10 Hz as reference value.

The synchrotron approach has been proven to allow for optimal tumor conformal irradiation and to be reliable under hospital operating conditions. One of the disadvantages of synchrotrons is their large size and cost, including extensive shielding, which qualifies this approach predominantly for larger hospitals with multiple treatment rooms (3–5). The potential for laser acceleration to replace synchrotron and its injector linac is hoped to lie in a significantly reduced system size and cost combined with possibly further advantages like less complicated irradiation schemes or easier realization of a gantry.

Since experimental data in the energy range of relevance are not yet available, a cautious approach is appropriate. In their highly critical review, Linz and Alonso have emphasized that the gap between a laboratory laser acceleration experiment and the complex demands to a clinical accelerator is still too large for a credible assessment [6]. Obviously, increasing the currently achievable energies to the needed level is not the only issue. Ion collection, angular and energy selection, energy and intensity reproducibility, operational reliability, and flexibility are crucial.

*Also at Gesellschaft für Schwerionenforschung (GSI), Planckstraße 1, 64291 Darmstadt, Germany. i.hofmann@gsi.de
†Also at Center for Applied Physics and Technology Peking University, Bejing 100871, China.

The focus of the present study is on collection, focusing (for example, by a solenoid), and transverse beam quality. Transverse focusing of laser produced protons close to targets was studied experimentally by different authors [7–9]; magnetic focusing (quadrupolar or solenoidal) was studied experimentally [10,11] and theoretically [12]. Therapy related studies so far have been constrained to our knowledge on the purely longitudinal energy selection issues. The details of the irradiation scheme—to be optimized to the specifics of laser acceleration—with the number of range (energy) steps and the combination with lateral scanning cannot, however, be defined without detailed modeling of beam collection and the resulting beam quality.

Concerning beam generation, we build on an explicit particle-in-cell (PIC) simulation, making use of the new concept of radiation pressure acceleration (RPA) [13–15]. These simulations provide a clear reference regarding laser and target parameters needed to meet therapy requirements as well as an ion phase space distribution just at the ion source. It should be clear that these new ways of ion acceleration are not yet confirmed experimentally. Presently, the field of developing adequate laser systems and optimal schemes for ion acceleration is subject to rapid changes and by no means in a mature stage. Nevertheless, this paper makes a first attempt to investigate beam production together with collection and focusing in a consistent framework. Though proton beams have been chosen here as paradigm, we emphasize that, alternatively, diamondlike carbon (DLC) foils producing pure carbon beams can be used as targets. This option has the advantage that DLC foils a few nanometer thick are already available (see e.g. [16]) and may be better suited for therapy applications.

We start with a summary of HIT parameters and basic particle requirements in Sec. II and discuss the RPA acceleration scheme in Sec. III. The achievable beam quality (emittance) based on collection by a solenoid is described by a scaling law in Sec. IV. In Sec. V we describe the impact on particle selection, and in Sec. VI we give a summary of results and an outlook.

II. PARTICLE REQUIREMENTS

A. HIT facility

The HIT facility uses primarily $^{12}C^{6+}$ beams due to their superior physical and biological efficiency compared with protons [5]. Their high linear energy transfer is their main advantage, but in HIT also protons are specified for reference to therapy centers using protons. For comparable physical dose protons require typically 40 times higher particle flux than carbon according to their lower energy transfer. The exact ratio is depending on the biological efficiency, which is more complex for carbon ions.

For a penetration range between 2 and 30 cm in water an energy variation between 85–430 MeV/u for carbon, and 50–220 MeV for protons in up to 254 energy steps is foreseen. Each energy is delivered by a 1–10 s long spill of a synchrotron cycle up to the required energy; even lower energies are generated by using passive range-shifting devices. In principle, energy steps with 1 mm range variations below 22 cm range, and 1.5 mm variation above are possible. In practice only about 50 energy steps are used, which is sufficient to deliver a spread-out Bragg peak (SOBP) for uniform dose deposition over the depth of the tumor with accuracy better than the required ±3%–5%. Besides an energy library an intensity library is used with 20 intensity steps and a ratio 1000:1 between maximum and minimum intensity.

B. Depth scanning

Combining lateral scanning with small step energy scanning as in HIT leads to a relatively complicated irradiation library, especially if a given energy does not cover a planar section of the tumor due to obstacles of different density, like bones. Therefore, Weber *et al.* have proposed a *depth scanning technique*, where the naturally small energy spread from a synchrotron is broadened by a wedge absorber to the extent that sufficient dose uniformity in a large tumor can be reached by overlaying only 5–10 individual (spread-out) Bragg curves [17]. This principle is shown schematically in Fig. 1. It is noted that uniform irradiation of a larger tumor requires the highest intensity in the top energy beam irradiating the distal layer, whereas lower energies benefit from the energy deposition of the higher energy beams and need reduced intensity. Such a scheme lends itself favorably to laser accelerated ions, which have naturally a large energy spread. For a 10 Hz laser system it is crucial to have as few energy steps and as large a diameter of the cylindrical voxel as are compatible with dose uniformity [17]. In practice however, as will be seen in the following section, the issue of depth dose

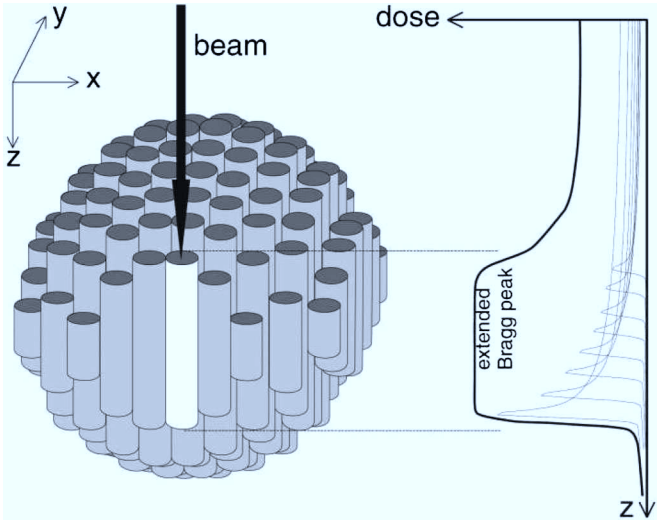

FIG. 1. Schematic principle of depth scanning with energy broadened ion beam (courtesy U. Weber).

uniformity sets clear limits to the tolerable energy spread. A larger transverse voxel size allows more efficient use of the abundance of particles in a laser accelerated bunch, again within the limits of transverse dose uniformity.

C. Particle fluence requirements

The particle fluence F (in [particles/cm^2]) is given by

$$F = 6 \times 10^8 D\rho(dE/dx)^{-1}, \quad (1)$$

where D is the dose [Gy], dE/dx is the linear energy transfer [keV/μm], and ρ the mass density [g/cm^3]. Following Ref. [18] a proton fluence of 10^9/cm^2 produces a dose of 3.2 Gy in the Bragg peak of a nearly monoenergetic beam at kinetic energy of 200 MeV, or 6.3×10^8/cm^2 are needed to reach a standard dose value of 2 Gy (to be used here as reference).

For a SOBP and given fluence, the peak dose drops with increasing energy width. In order to quantify this effect we have calculated depth dose distributions with a simplified analytic approximation to the model used in Ref. [18], which is based on pencil beams in water, and superimposed contributions from different energies within a given width. Results for proton fluences of 10^9/cm^2 are shown in Fig. 2 for flat energy profiles of different widths around the reference energy of 200 MeV, including a case of Gaussian energy distribution with FWHM width of $\pm 10\%$. It is noted from Fig. 2 that broadening to $\pm 10\%$ leads to a peak dose reduction by a factor 2, or even more for the Gaussian energy profile. Loss of the sharp Bragg peak edge for broadened energy distributions may, however, not be acceptable for the distal layer at the top energy. We therefore assume typically $\pm 1\%$ energy width for the distal layer and thus require a proton fluence of 7×10^8/cm^2, or an equivalent number of 1.8×10^7/cm^2 carbon ions to reach the standard 2 Gy dose value. For a SOBP with Gaussian beam at FWHM energy width of 10%, the 2 Gy dose requires a proton fluence of 1.7×10^9/cm^2, or an equivalent number of 4.2×10^7/cm^2 carbon ions.

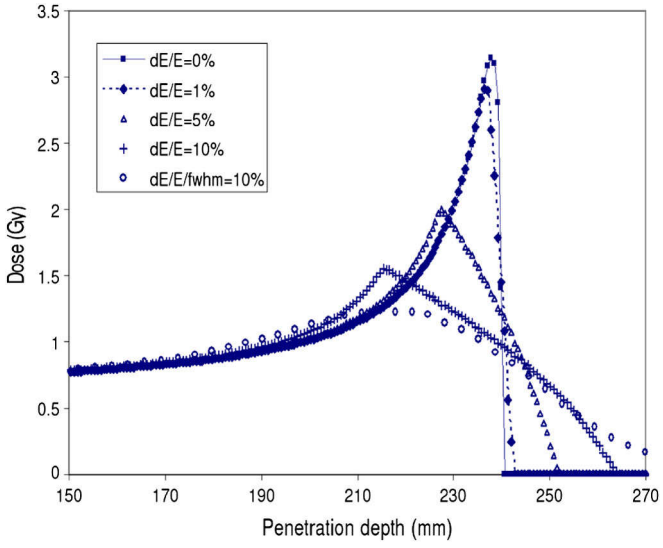

FIG. 2. Depth dose profiles for protons in water with initial fluences 10^9/cm^2 and different incoming energy widths (0 ... $\pm$ 10%).

For laser acceleration and depth scanning with 1 cm^2 spot area as reference value, the required corresponding peak bunch intensity is then 7×10^8 protons, or 1.8×10^7 carbon ions. For an assumed total area of 10×10 cm^2 this results in a peak total particle flux of 7×10^{10} protons or 1.8×10^9 carbon ions in the distal layer. In case of a synchrotron this is provided by a complete spill (of typically 10 s duration) at this energy, which is scanned over all transverse voxels; lower energy layers require less particles due to Bragg peak overlap in the entrance channel.

III. LASER ACCELERATION

At focused intensities beyond 10^{18} W/cm^2, laser pulses can produce particle beams. On solid targets, such pulses first produce relativistic electrons, which may transfer energy to ions in a secondary step, mediated by space charge fields. There are different regimes of ion acceleration depending on target thickness and laser parameters. Here we briefly discuss target normal sheath acceleration (TNSA), which is best investigated presently, and then discuss more recent results based on radiation pressure acceleration (RPA), which is by far the more efficient mechanism of ion acceleration.

It is important to understand that charge separation in solids leads to huge electric fields in the order of TV/cm, and ions can achieve GeV energies over distances of a few micrometer, i.e., within the Rayleigh length of the focused laser beam. Hence, on the scale of an ion therapy device, ion acceleration takes place in an almost pointlike volume.

A. Laser ion acceleration by TNSA

The TNSA mechanism works for relatively thick targets (e.g. μm thick Al foils). Relativistic electrons generated at the irradiated surface spread through the foil and build up high electrostatic fields when emerging from the rear surface. These fields accelerate surface ions (often hydrogen contaminants), producing dense short ion beam pulses that typically have low emittance, but also broad energy spectra. Maximum proton energies of up to 60 MeV (cutoff energy of an exponential spectrum) have been observed in 2000 [1]. This record value has not been exceeded since then. The efficiency of laser-to-ion energy conversion is of the order of 1% or less. For TNSA scaling considerations predict that laser intensities of a few 10^{22} W/cm^2 are required to reach the 200 MeV proton energies of interest for ion therapy [19]. Various methods have been proposed to obtain peaked energy spectra, mainly by restricting the ion source to small volumes over which the accelerating

field is homogeneous [3]. These methods suffer from lower conversion efficiency and particle flux.

B. Radiation pressure acceleration and its scaling relations

Ions are also accelerated at the irradiated front side of the targets, where the radiation pressure pushes electrons inwards relative to the ions, thus creating the field that accelerates the ions. The basic mechanism is illustrated in Fig. 3. The laser is focused on the target from the left side; protons or ions are accelerated to the right, where the required particle optics is placed. The radiation pressure compresses the electrons inside the target foil, until balance with the charge separation electric field is reached. At this point, there is a significant difference between linear and circular polarized light. For linear polarization, the light pressure beats with twice the laser frequency and causes large-amplitude electron oscillations in longitudinal direction. This strongly heats the electrons since they pick up the laser ponderomotive energy stochastically many times (see basic theory discussed in [20] and the very instructive movie animation given in [21]). On the other hand, circular polarization produces a quasistationary radiation pressure, gently pushing the electrons in laser direction and keeping them cool. This is called phase-stable acceleration, because the phase between electrons and light stays almost constant in contrast to linear polarization. As a result the light pulse acts like a piston that accelerates the foil as a whole, with ions coupled to electrons by the electrostatic field. After a short period of initialization, acceleration proceeds in a ballistic mode that leads to a quasimonochromatic ion energy spectrum and high efficiency of laser-to-ion energy conversion.

Phase-stable radiation pressure acceleration using circular polarized light (RPA) can be modeled in simple analytical terms (see Ref. [15]), as long as one-dimensional (1D) geometry is assumed. Momentum balance $\rho d v_i = 2I_0 t/c$ determines the foil velocity v_i after time t; here ρd is the areal density of the foil, $2I_0/c$ the radiation pressure, I_0 the laser intensity, and c the velocity of light. The foil thickness should not be thinner than the distance of charge separation, such that the compressed electrons still reside inside the ion volume. This leads to the estimates of optimal foil thickness $d \approx (2c/\omega_{pi})(I_0/\rho c^3)^{1/2}$ and of ion energy

$$\epsilon_i/(m_i c^2) \approx k(I_0/\rho c^3)(\omega_{pi} t)^2, \tag{2}$$

where k is a number of order unity, m_i the ion mass, $\omega_{pi} = (e^2 n_i/\epsilon_0 m_i)^{1/2}$ the ion plasma frequency, and $n_i = \rho/m_i$ the ion density. The scaling of ion energy with laser intensity depends on the time period available for acceleration. If t is given by the lifetime of the ion bunch ($\omega_{pi} t \approx 1$), the maximum ion energy scales linearly with intensity. However, the phase-stable mode of acceleration is also limited by the bending of the target foil, occurring when the laser pulse pushes a disk out of the foil that has a diameter of 2σ, the laser focus diameter. Effective acceleration then stops after about a distance σ of propagation. This implies an acceleration time given by $(\omega_{pi} t)^2 \sim (\sigma\omega_{pi}/c)/(I_0/c^3)^{1/2}$, and the scaling $\epsilon_i/m_i c^2 \sim (\sigma\omega_{pi}/c)(I_0/c^3)^{1/2}$ of the maximum ion energy is obtained. In Fig. 4, these scalings are compared with actual 2D PIC simulations. It is seen that the model estimates put an upper and a lower limit on what can be actually achieved.

Experimental verification of the RPA regime is still in its beginnings. Major challenges are to fabricate the required ultrathin target foils, that have a typical thickness in the order of 10 nm only, and to generate laser pulses rising very steeply at their front edge. Contrast ratios of 10^{-11} and better are required in order not to destroy the target foils prematurely. Irradiating 30 nm thick carbon foils with an

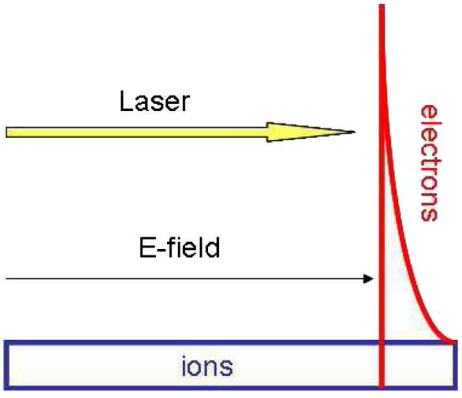

FIG. 3. Schematic drawing of electron and ion densities after some femtoseconds of laser irradiation for radiation pressure acceleration (RPA). Compression of electrons by radiation pressure occurs until balance with the charge separation electric field is reached, which accelerates foil ions as a whole.

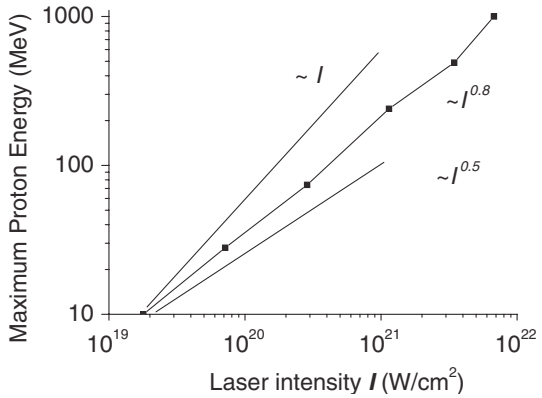

FIG. 4. Maximum proton energy versus laser intensity. The black squares represent results from the 2D-PIC simulations described below; they follow an effective scaling of $\epsilon_i \sim I_0^{0.8}$. The upper and lower model limits are shown for comparison.

80 J, 100 TW laser pulse at intensities of 10^{20} W/cm^2 and achieving 10^{-11} contrast, 185 MeV [22] and even 500 MeV C^{6+} ions [23] have been obtained. In another experiment characteristic features of the RPA regime such as a peaked energy spectrum and high laser-to-ion energy transfer could be confirmed [16]. These are first steps to demonstrate the feasibility of the RPA approach for ion beam generation. In particular, carbon beams, best suited for ion therapy, are favored, because rather stable diamondlike-carbon (DLC) layers are now available to provide the ultrathin target foils. Here we restrict ourselves, nevertheless, primarily to proton beams for an exploratory discussion. Yet we show that our main results can be directly applied to carbon beams as well.

C. Self-organizing regime of RPA

Recently a self-organizing regime of RPA has been identified that allows for longer periods of phase-stable acceleration (see Ref. [24]). In this regime the target foil becomes transparent to the light in the wings of the accelerated disk, and only a central part of the disk, a few laser wavelengths in diameter, is then accelerated in a more stable way. Ideally the acceleration interval is limited by lateral Coulomb expansion given by $\omega_{pi}t \approx 1$, and the maximum ion energy would scale $\propto I$ according to Eq. (2). The 2D-PIC simulations shown in Fig. 4 indicate that the actual scaling is more like $\propto I^{0.8}$ and that a laser intensity of about 10^{21} W/cm^2 is sufficient to produce the 200 MeV protons required for ion therapy.

D. Parameters for 200 MeV protons

In the simulations, we have taken a circular polarized laser pulse with wavelength $\lambda = 1$ μm and maximum normalized vector potential $a = eA/mc^2 = 35$, corresponding to an intensity of $I = 1.37 \times 10^{18}$ W/cm$^2 \cdot 2a^2/\lambda^2$. The pulse has a Gaussian radial profile with $2\sigma = 20\lambda$ full width at half maximum and a trapezoidal shape longitudinally with 20λ flattop and 1λ ramps on both sides. It is normally incident on a uniform, fully ionized hydrogen foil of thickness $D = 0.4\lambda$ and normalized density $N = n_e/n_{\mathrm{crit}} = 80$, where the electron density n_e is given in units of the critical density $n_{\mathrm{crit}} = \pi m_e c^2/\lambda^2$. The size of the simulation box is $50\lambda \times 80\lambda$ in (x, y) directions, respectively. We take 100 particles per cell per species and a cell size of $\lambda/80$. Periodic boundary conditions are used for particles and fields in transverse direction, and fields are absorbed at the boundaries in longitudinal direction.

Here we summarize the laser parameters: (i) Spot radius 10 μm; (ii) pulse duration 66 fs; (iii) specific power 3×10^{21} W/cm^2; (iv) peak power 10 PW; (v) pulse energy 620 J; (vi) average power 6 kW (10 Hz).

Note that peak and average power as well as pulse energy would ideally drop by a factor 4, if a 5 μm radius spot could be realized without harming the underlying acceleration mechanism.

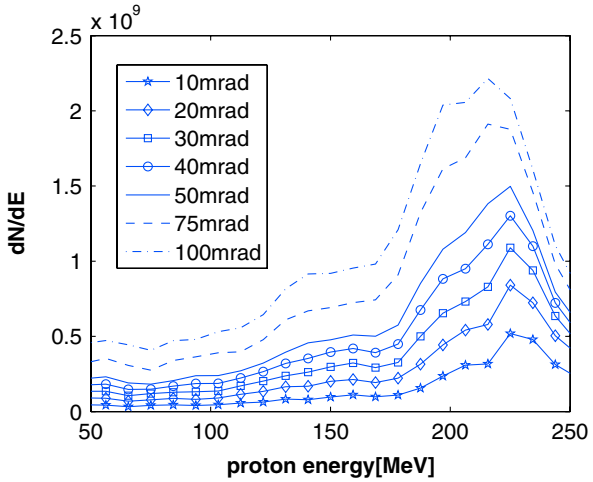

FIG. 5. Spectral yield of protons as a function of energy and for different production cone angles.

E. Spectral yield

In order to evaluate the transport properties of the proton output, we find it useful to consider the spectral yield of particles as function of energy E and a given production cone angle Ω,

$$\frac{dN(E, \Omega)}{dE}[\mathrm{MeV}^{-1}], \tag{3}$$

which describes the number of particles in a small energy interval dE and within a cone angle $\pm\Omega$. The proton spectrum for the parameters given above is plotted in Fig. 5. The energy distribution is "quasimonoenergetic" with a pronounced peak at about 225 MeV. The rising slope to the left of the maximum is favorable for achieving a uniform depth dose distribution, where the higher energies require higher intensity.

IV. ION COLLIMATION OR COLLECTION

A suitable irradiation scheme requires definition of an energy window matching a desired range depth as well as transverse divergence and size. We therefore require detailed information on the expected final 6D phase space distribution, which differs substantially from the source production spectral yield. In principle, two distinct approaches can be discussed: a pure (ballistic) aperture collimation up to the tumor, or a lens focusing collection and subsequent transport.

Aperture collimation.—As an example, we refer to a scheme considered in Ref. [25] with the goal of a very compact particle selection not requiring much more than 1 m distance laser target to tumor. This proposal assumes transverse collimation by a small aperture immediately behind the target limiting transmission to a production cone angle of $\Omega \approx \pm 10$ mrad (0.5 degrees), which makes the transverse beam radius grow by 10 mm per meter distance; it is followed by a dispersive energy separation

device and a second collimating aperture close to the tumor. Obviously, the available particle flux density from the source and the need for keeping the distance low are critical issues here.

Lens collection.—Significantly more flexibility can be expected, if active lens focusing (by a solenoid or quadrupoles) is applied, which allows using a larger production cone angle. The final beam size is in principle independent of distance and determined primarily by the achievable beam emittance.

A. Emittance and energy spread

The transverse emittance ϵ of a beam originating from a source spot of radius r_0 and filling uniformly an angular cone with maximum spatial angle $\Omega_{\max}$ is given as

$$\epsilon \equiv r_0 \Omega_{\max}, \tag{4}$$

where it is assumed that the $x - x'$ and $y - y'$ phase planes ($\prime \equiv d/ds$, with s the distance) are each filled within—here upright—elliptical boundaries. Hence, the emittances are defined as areas of these ellipses (divided by π). For more general distributions these geometrically defined emittances are often replaced by rms values. In our study we use a truncated Gaussian phase space distribution and define "total emittances"—related to as emittances—as areas (divided by π) of an ellipse containing 95% of particles. The source emittances are typically quite small in our case. With $r_0 \approx 10$ μm and $\Omega_{\max} \approx 50$ mrad, for example, we obtain $\epsilon \approx 0.5$ mm mrad.

A drift or transformation through a linear focusing lens results in a rotation of the phase ellipses in $x - x'$ and $y - y'$, and a distortion for nonlinear lens action. For particles at fixed energy the enclosed areas remain invariant, which expresses the validity of Liouville in 2D phase space; or in 4D transverse phase space, if coupling forces exist. The concept of invariant emittances or phase space areas in any 2D phase plane, however, makes sense only for a specific energy. The large production energy spread leads to a longitudinal expansion, and during expansion the different energies become correlated with different positions along the bunch. This debunching or bunch spreading is proportional to the intrinsic energy spread and to distance.

These different energy sections, however, rotate differently within a collector lens, which has a focal length depending on energy. The volume in a 6D transverse-longitudinal phase space still remains constant. A projection of this transverse-longitudinal phase space onto the reduced 4D or 2D transverse phase space, however, destroys this energy correlation and shows an effective growth of this *chromatic emittance*. Practically speaking, it is not possible to disentangle the energy correlation at any later stage. This would require a highly time-resolved resolution on a sub-ns time scale. Averaged over the duration of the bunch, the practically relevant emittance therefore is the *chromatic* one.

B. Solenoid collector

Laser acceleration has in common with other sources of "secondary particles" (antiprotons, muons, etc.) that a collector lens is advantageous to focus particles born under different angles and energies into the acceptance of any subsequent beam transport or processing system.

Quadrupolar lenses can provide large gradients in one plane, but the defocusing action in the other plane easily leads to large apertures and saturation problems of pole tip fields. For antiproton collection cylindrical magnetic lenses have come into practice, where the field is produced by currents through cylindrical conductors. One example is lithium lenses, where a uniform current flows through a rod of lithium and generates a field proportional to r; alternatively, in the "magnetic horn" the cylindrical current flow is through an outer (cylindrical) and an inner (approximately parabolically shaped) conductor, which the particles must necessarily traverse under a relatively small angle. Crossing of conductors is, however, not feasible for the relatively low energies of protons or ions for medical applications, therefore we concentrate here on the option of a rotationally symmetric magnetic field from a solenoid magnet as reference basis. A quadrupole based focusing system could still be a practical choice, if very small and preferably asymmetric (in x and y) production angles are taken to get a better match to the asymmetric quadrupole focusing. We assume that the distance target to solenoid or first quadrupole is—at this point arbitrarily—chosen to be 240 mm. For the rest of this study we concentrate on the case of a 360 mm long solenoid.

For the simulations in Sec. IV C, we need the fully 3D magnetic field for the sample solenoid. The field was calculated from Biot-Savart's law on a mesh in r, z with 0.5 mm mesh width. The inner diameter was 44 mm, the

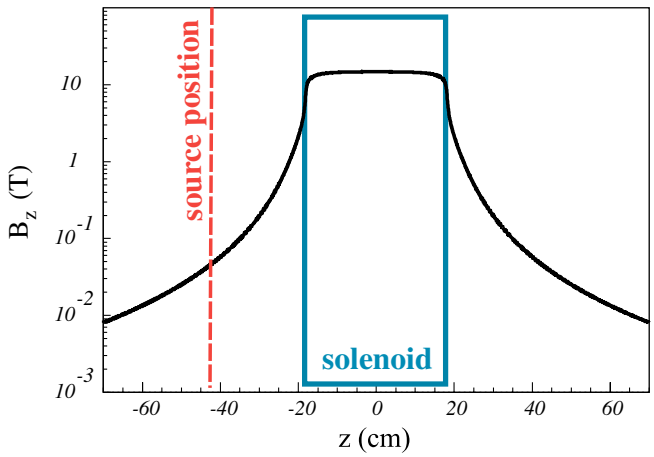

FIG. 6. Calculated values of B_z through solenoid versus distance.

outer 76 mm [26]. The maximum field needed to create a focal distance of 1 m for 200 MeV protons was found 10 T in the center of the solenoid. The calculated field distribution is shown in Fig. 6.

C. Chromatic emittance growth

In order to examine the growth of the chromatic emittance quantitatively for a given collector—here the above defined solenoid—we have employed the DYNAMION code [27], which allows tracking through an externally provided field configuration and includes higher order effects in amplitudes, the dependence of focusing on energy as well as space charge effects. The latter are based on particle-particle interaction in DYNAMION, which limits the space charge resolution, but it is found that for the present study space charge is not a critical issue.

The initial beam at the production target is assumed to have Gaussian real space and angular distributions truncated at 2σ. The initial pulse duration is set to 140 ps. Starting from such a relatively long initial proton bunch duration rather than the sub-ps starting value—as given by the laser pulse duration—means ignoring the complex dynamics of the very early expansion of the proton cloud and assuming its full space charge neutralization and a simple ballistic motion up to this point. The early charge neutralization and deneutralization phase is beyond the scope of our study and requires different simulation tools.

While the size of the production laser focal spot is always taken as 10 μm (for 2σ), we study different subsets of particles out of the total production spectrum in angle and energy as indicated in Fig. 5. These subsets are defined by Gaussian distributions of transverse angles up to maximum values (truncated at 2σ) of $\pm\Omega$; similarly, we assume the subsets are constrained to an energy window of $\pm\Delta E/E$ around the central proton energy of 200 MeV, which is varied up to ± 0.05. The distance source to solenoid is chosen as 240 mm, with the strength of the solenoid magnetic field adjusted to create a focal spot at 1 m. The source stand-off distance and focal distance are relatively uncritical at this point, except for the fact that larger values would require somewhat lower solenoid magnetic field and lead to slightly reduced chromatic aberrations.

In Fig. 7 we show representative orbits for $\Omega = \pm 40$ mrad and $\Delta E/E = \pm 0.05$ and ignoring space charge effects. Note that the approximately 3 mm diameter waist at $z \approx 1700$ mm is a result of the increased chromatic emittance due to the dependence of focal length of the solenoid on particle energy and mixing over all particles of the ensemble. For a monochromatic beam it would be significantly smaller (note that the piecewise straight trajectories are only a plotting artifact of DYNAMION, which provides output data only at the solenoid edges and midpoint).

At the trajectory crossover close to 1700 mm a projection into the $x - x'$ phase space shows in Fig. 8 the

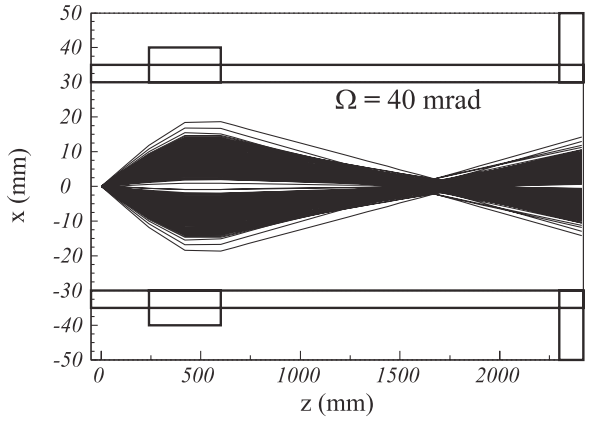

FIG. 7. Sample trajectories through solenoid collector and $\Delta E/E = \pm 0.05$.

different rotation in phase space for different energy slices, where bunch tail particles (lower energy) are ahead in the (clockwise) rotation. The ellipse indicates the emittance including 95% of particles. Figure 8 also indicates that the 95% emittance is a somewhat pessimistic definition, since the hourglass shape of the distribution has a strong concentration of density in the center. Discarding a larger fraction of particles leads to smaller values of emittances. The 85% emittance, for example, is only about 1/2 of the 95% emittance.

The dependence on the energy width is shown in Fig. 9, always based on the 95% emittance. A linear behavior is found for $\Delta E/E > 0.01$. Below this value emittances saturate at a finite level—here about 3 mm mrad, which can be explained as residual geometric aberration and nonparaxial

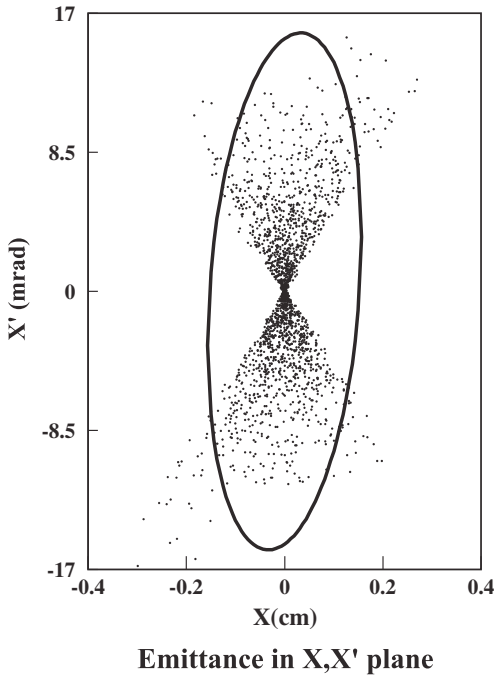

FIG. 8. Phase space projection at crossover ($\Omega = 40$ mrad).

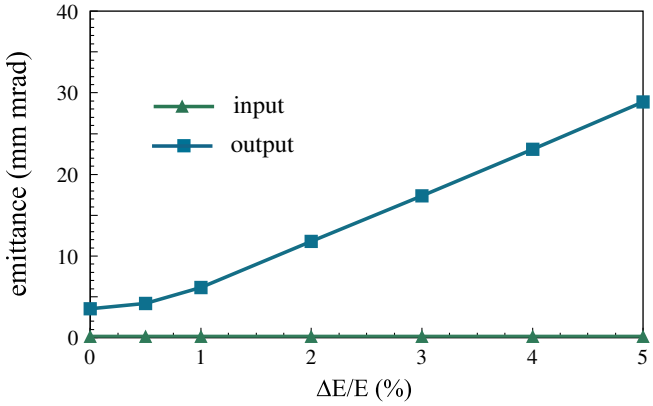

FIG. 9. Emittances for variable $\Delta E/E$ ($\Omega = 43$ mrad).

effect due to the relatively large transverse angle. This effect vanishes for small angles.

Results of emittances for different production cone angles up to $\Omega = 43$ mrad (2.3°) are shown in Fig. 10. A quadratic dependence on the initial cone angle is readily confirmed.

These findings suggest an emittance scaling law for the chromatic emittance of the following form:

$$\epsilon = \alpha_c \Omega^2 \frac{\Delta E}{E}, \tag{5}$$

where α_c is a constant for a given geometry and in our case $\alpha_c \approx 0.3$ m/rad. It is found to increase with increasing dimensions that lead to larger beam excursions, like the solenoid length and the stand-off distance target to solenoid. For an equivalent quadrupole triplet focusing the much larger beam excursions equally cause larger α_c, but the form of the scaling law remains unchanged. Equation (5) is the basis for a quantitative discussion of achievable beam quality after collection.

Note that the α_c also depends on our choice of a 95% fractional emittance. By using smaller fractions, like 85%, the α_c would drop by a factor 2 as does the emittance. We prefer, however, to remain on the conservative side in case further studies show that a final scatter foil is needed to smear out the highly structured phase space of Fig. 8. Such a structure might be detrimental to the desirable high real space uniformity on the tumor.

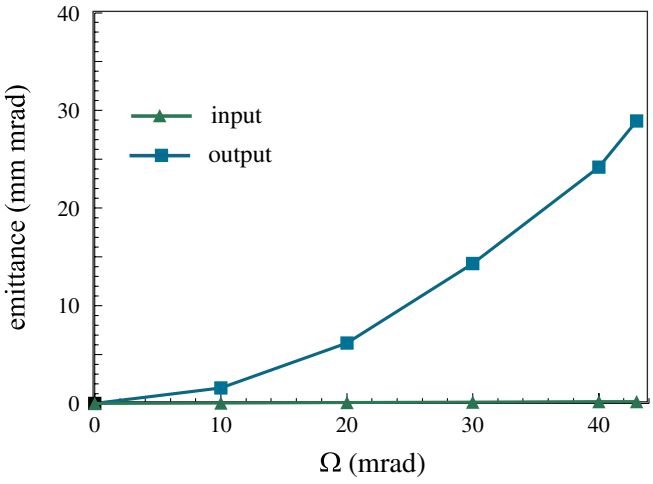

FIG. 10. Emittances for different opening angles into solenoid ($\Delta E/E = \pm 0.05$).

Space charge effects are a relatively small correction for the above simulations, which we have estimated for one example. According to Fig. 5 the number of protons within a typical cone angle of $\Omega = 15$ mrad and $\Delta E/E = \pm 0.05$ is 6×10^9. At this level of intensity we have found that the shift of focal length due to space charge is only 10% of that caused by the energy spread. A more complete simulation of the effect of space charge—including the full production spectrum of protons rather than a sample selected in energy and angle as well as initial deneutralization effects—is left for future work.

V. PARTICLE SELECTION

A. Required emittance and usable intensity

Beam transport and focusing of particles on the tumor require a beam not exceeding a certain upper limit of emittance—here the chromatic emittance—that needs to be defined according to the final transfer optics. The tolerable value—for simplicity called "required emittance"—is the smaller the larger the distance of final optics from the tumor and the smaller the desired spot size. Once the required emittance is defined, combinations of the energy window $\Delta E/E$ and production cone angle Ω consistent with it are defined by Eq. (5). These combinations, on the other hand, determine the available number of particles according to Fig. 5, here simply called "usable intensity." We find it convenient to display the usable intensities by color codes in a contour plot in the plane of $\Delta E/E$ and Ω as shown in Fig. 11. We also include two lines (in red) of exemplary values for the required emittances, both satisfying Eq. (5). Only values of $\Delta E/E$ and Ω *under* the required emittance curves are tolerable—points above would exceed the predefined value of required emittance.

Three exemplary cases can be discussed.

Aperture collimation.—For pure aperture collimation as discussed in Sec. IV we can ignore Eq. (5). For a spatial angle $\Omega = 10$ mrad the simulation predicted proton yield according to Fig. 5 is $dN(E,\Omega)/dE \approx 0.25 \times 10^{-9}$ [MeV^{-1}] (with range of energy windows of interest marked by an ellipse in Fig. 11). Assuming that a small energy window of $\Delta E/E \approx \pm 0.01$ is needed for a sharp Bragg peak at the distal layer (see Sec. II C), the usable intensity is calculated as 10^9. The standard proton fluence of 7×10^8/cm^2 required at the distal layer with a spot radius of 10 mm (resulting at 1 m distance according to the assumed divergence) requires, however, 2×10^9, which would be missed by a factor of 2 for a single laser shot. This missing factor grows quadratically with the distance source target; likewise there is no room for a safety margin

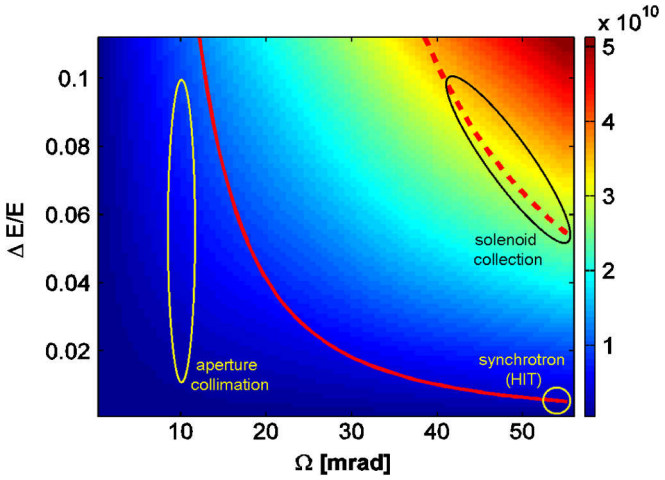

FIG. 11. Contour plots for usable intensities of 200 MeV protons as a function of selected production cone angle and energy window, with curves of two examples for constant chromatic emittance (required emittance) (red solid: $\epsilon = 5$ mm mrad; red dashed: $\epsilon = 50$ mm mrad).

to respond to uncertainties in acceleration mechanism, limitations in available laser energy, etc.

Solenoid collection.—Here we assume $\epsilon = 50$ mm mrad for the required emittance, which is an order of magnitude above common values for synchrotrons as in the HIT facility (dashed red line in Fig. 11, with black ellipse marking a practical range of $\Delta E/E$ for SOBP's). This relatively large value of emittance is justified by two assumptions: first, the distance of transport to the patient can be minimized due to absence of a large gantry system; second, the spot size can be chosen larger than for a synchrotron solution due to the abundance of particles. An increased spot size is also in the interest of utilizing as many ions per bunch as possible in order to keep the total number of pulses as low as possible. According to Fig. 11 the particle yield consistent with $\epsilon = 50$ mm mrad can be as high as 3.5×10^{10} particles for $\Delta E/E = \pm 0.1$ and $\Omega = 40$ mrad, which is 20× the fluence requirement of $1.7 \times 10^9/\text{cm}^2$. For $\Delta E/E = \pm 0.01$, and assuming again $\Omega = 40$ mrad, the usable intensity (roughly proportional to the energy width) drops to 3.5×10^9, which is 5× the fluence requirement of $7 \times 10^8/\text{cm}^2$. Using $\Omega = 100$ mrad we can still expect 8×10^9 particles according to Fig. 5, which is 11× the fluence requirement. Hence, in all cases the usable intensities from our simulation can be at least 1 order of magnitude above the required proton fluences, and enough flexibility and safety margin (in terms of simulation predictability) is provided.

Comparison with synchrotron beams (HIT).—The example $\epsilon = 5$ mm mrad (solid line in Fig. 11) would correspond to the mean value of horizontal and vertical emittances specified for HIT and is shown here only for comparison. This small emittance is required in HIT for final transport through the full gantry system as well as transverse scanning on a small 2–5 mm spot radius. Simultaneously a small energy spread of ± 0.004 is needed to maintain beam quality throughout bending in the gantry. Our simulation predicts $\approx 2 \times 10^9$ particles to meet simultaneously this emittance value and the small energy window, provided that the production cone angle is chosen as large as $\Omega = 50$–60 mrad. In this sense the quality of beam from laser acceleration is even competitive with that of a synchrotron solution. On the upper end of the curve, at $\Delta E/E = \pm 0.1$ and $\Omega = 12$ mrad, the same emittance holds, but the predicted intensity rises to even 10^{10} particles.

B. Remarks on energy and intensity selection

The above maximum achievable intensities for the laser accelerated particles have to be compared with the peak requirements for depth scanning. A practical scheme could employ a sequence of 5–10 energy steps to carry out irradiation of a given cylindrical voxel of 1 cm^2 area, with decreasing intensities for the lower energies tailored to achieve a uniform depth scanning as indicated in Fig. 1. As indicated in Fig. 2, the allowed energy widths are likely to vary between 1% and 5%–10% in order to achieve the required dose uniformity on the one hand and keep the number of energy steps as low as possible on the other hand. Since the production spectrum in Fig. 5 is always much broader an energy filter will be required. This could, for example, consist of a conventional dispersive system using a bending magnet similar to the one suggested in Ref. [25]. Hence, variation of the bending field—in parallel with the solenoid focusing field—can determine the selected center and width of an energy window. The additional requirement on intensity per pulse must then be fulfilled by an independent control, which could be a laser variation or a beam optics degrader via defocusing. These selection issues clearly require careful future studies.

We can thus attempt a rough estimate of the total number of laser pulses: for a 10×10 cm^2 tumor this would require at least 500–1000 beam pulses per side delivered in 50–100 s, or 100–200 s for both sides (one fraction).

At this point we have assumed that each pulse matches the required dose accuracy of >95%, which cannot be expected from a laser acceleration source by current experience. On the other hand, the sub-ns scale duration of the laser generated ion pulses does not allow in-flight intensity correction as with the slow synchrotron spill. Therefore, the nominal intensity has to be approached by a sequence of correction shots with fractions of the nominal intensity. For an assumed error of ±30% per shot, we estimate an average increase of the irradiation time by at least a factor 3, which would raise the total irradiation time to an acceptable duration of 10 min.

C. Carbon ions versus protons

The equivalent model simulation as in Sec. III C, but for carbon ions at 400 MeV/u requires a factor 10 higher laser

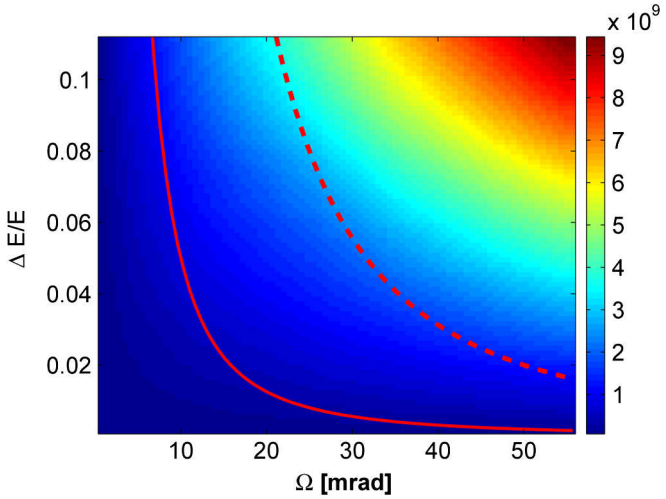

FIG. 12. Contour plots for usable intensities of 400 MeV/u carbon ions with curves of constant chromatic emittance.

power and energy per shot and has resulted in a particle yield distribution as shown in Fig. 12, again with the lines of constant emittance as in Fig. 11 (solid: $\epsilon = 5$ mm mrad; dashed: $\epsilon = 50$ mm mrad).

The output of particles relative to the $\epsilon = 50$ mm mrad line is about a factor of 20 below the proton output in terms of number of ions. Note that the lines are shifted as we have assumed $\alpha_c = 1$—over a factor 3 larger than for protons—to account approximately for the (estimated) effect of a longer solenoid as needed for focusing ions with a 3 times larger magnetic rigidity. Keeping in mind that carbon ions have a 40 times higher biological efficiency compared with protons of the relevant energy, there is an additional margin of a factor 2, and all observations made for the proton case equally apply.

VI. SUMMARY AND OUTLOOK

Results of our point study have demonstrated that intensities and beam qualities expected from the output of laser acceleration simulations—using the self-organizing regime of RPA and idealized conditions—and collected by a solenoid lens are quite compatible with the requirements for irradiation of large tumors. Based on our simulations for particle production and chromatic emittance estimates, the following observations can be made: (i) Although laser acceleration produces, generally speaking, copious amounts of protons/ions the spectral distribution sets limitations and needs to be carefully examined. (ii) A magnetic particle collection system (with solenoid or quadrupole focusing) is advantageous, while pure aperture collimation discussed primarily in the literature appears to be undesirably limited in particle intensity and allows only insufficient use of the produced particles. (iii) In spite of its finite chromatic effect, a solenoid collector is able to select over an order of magnitude more particles into the required phase space volume (emittance *and* energy spread) than actually needed—up to 10% of the total production. (iv) The relatively low utilization of the actual yield ($< 1\%$) leaves enough margin and calls for an optimization of laser and production target; up to an order of magnitude less particle yield than predicted by our simulation would still be acceptable and attractive at the same time in terms of possibly cost saving on the side of the laser and the required shielding. (v) By using the solenoid focusing—instead of aperture collimation—the actual distance laser source to irradiation target appears not a critical issue and should leave enough flexibility to accommodate steering, an energy selection system and the necessary shielding (probably still demanding for the higher magnetic rigidity carbon ions). (vi) Depth scanning using typically 5–10 energy steps is favored; the detailed realization of an energy selection system maintaining uniform irradiation depth profiles needs to be examined in future work. (vii) Provisions have to be made (for instance, by a transverse scatterer following the energy selection) to ensure a sufficiently uniform transverse distribution. (viii) Correction shots to reach a dose accuracy of $>95\%$ may be needed, which would bring the total irradiation time per fraction up to approximately 10 min—based on a 10 Hz laser system and $\pm 30\%$ intensity uncertainty per shot. (ix) Laser requirements for protons based on a 10 μm radius spot with 10 PW peak power, 400 J pulse energy, and 4 kW average power (10 Hz) are about a factor 5–10 beyond the current state of the art, hence such a development is most urgently required for experimental verification.

The present study on beam quality of laser accelerated particles is only one of a number of necessary conditions to be fulfilled in order to render laser acceleration a viable approach for therapy. Experimental data on laser accelerated particles in the energy range needed, their quality, and reproducibility are as crucial as is the technical realization of the required laser system and its price. More detailed studies on complete transport as well as energy and particle selection systems tailored to match with the irradiation requirements will have to be carried out to further advance the assessment of laser acceleration compatibility with tumor irradiation. Obviously, the total irradiation times per fraction estimated here could be made shorter, if higher repetition rate laser systems were available. But the average power determining largely the cost of the laser system would equally go up, unless this can be balanced by an optimization of laser and target towards lower single shot energy and a desirable reduced particle yield per shot. All these issues are subject to the outcome of future experimental and careful system studies.

[1] R. A. Snavely *et al.*, Phys. Rev. Lett. **85**, 2945 (2000).
[2] P. McKenna, Phys. Rev. E **70**, 036405 (2004).

[3] B. M. Hegelich *et al.*, Nature (London) **439**, 441 (2006).
[4] T. Haberer, W. Becher, D. Schardt, and G. Kraft, Nucl. Instrum. Methods Phys. Res., Sect. A **330**, 296 (1993).
[5] T. Haberer *et al.*, Radiotherapy Oncol. **73**, S186 (2004).
[6] U. Linz and J. Alonso, Phys. Rev. ST Accel. Beams **10**, 094801 (2007).
[7] P. K. Patel *et al.*, Phys. Rev. Lett. **91**, 125004 (2003).
[8] T. Toncian *et al.*, Science **312**, 410 (2006).
[9] S. Kar *et al.*, Phys. Rev. Lett. **100**, 225004 (2008).
[10] M. Schollmeier *et al.*, Phys. Rev. Lett. **101**, 055004 (2008).
[11] K. Harres *et al.*, Phys. Plasmas **15**, 056709 (2008).
[12] I. Hofmann *et al.*, Proceedings of HIAT09, Venice (2009), http://accelconf.web.cern.ch/AccelConf/HIAT2009/index.htm.
[13] T. Esirkepov *et al.*, Phys. Rev. Lett. **92**, 175003 (2004).
[14] A. Macchi *et al.*, Phys. Rev. Lett. **94**, 165003 (2005); X. Zhang *et al.*, Phys. Plasmas **14**, 123108 (2007); X. Q. Yan *et al.*, Phys. Rev. Lett. **100**, 135003 (2008); A. P. L. Robinson *et al.*, New J. Phys. **10**, 013021 (2008).
[15] O. Klimo *et al.* Phys. Rev. ST Accel. Beams **11**, 031301 (2008).
[16] A. Henig *et al.*, Phys. Rev. Lett. **103**, 245003 (2009).
[17] U. Weber, W. W. Becher, and G. Kraft, Phys. Med. Biol. **45**, 3627 (2000).
[18] P. Kundrat, Phys. Med. Biol. **52**, 6813 (2007).
[19] J. Fuchs *et al.*, Phys. Rev. Lett. **99**, 015002 (2007).
[20] P. Mulser, D. Bauer, and H. Ruhl, Phys. Rev. Lett. **101**, 225002 (2008).
[21] S. G. Rykovanov *et al.*, New J. Phys. **10**, 113005 (2008).
[22] A. Henig *et al.*, Phys. Rev. Lett. **103**, 045002 (2009).
[23] A. Henig, Ph.D. thesis, Munich University, 2010.
[24] X. Q. Yan *et al.*, Phys. Rev. Lett. **103**, 135001 (2009).
[25] C.-M. Ma, Laser Phys. **16**, 639 (2006).
[26] M. Droba (private communication).
[27] S. Yaramishev *et al.*, Nucl. Instrum. Methods Phys. Res., Sect. A **558**, 90 (2006).